Biosensors and Bioelectronics 47 (2013) 429–435

Contents lists available at SciVerse ScienceDirect

Biosensors and Bioelectronics

journal homepage: www.elsevier.com/locate/bios

Xanthine biosensor based on the direct oxidation of xanthine at an electrogenerated oligomer film

Shaolin Mu*, Qiaofang Shi

Department of Chemistry, Yangzhou University, Yangzhou 225002, Jiangsu Province, PR China

ARTICLE INFO

Article history:
Received 11 January 2013
Received in revised form
1 March 2013
Accepted 14 March 2013
Available online 26 March 2013

Keywords:
Poly(*o*-aminophenol-*co*-pyrogallol)
oligomer
Oligomer characterization
Reduced graphene oxide
Novel xanthine catalyst
Xanthine biosensor

ABSTRACT

Poly(*o*-aminophenol-*co*-pyrogallol) (PAP) was first synthesized via the electrochemical copolymerization of *o*-aminophenol and pyrogallol in the acidic solution, using a reduced graphene oxide/glassy carbon (RGO/GC) electrode as a working electrode. Reduced graphene oxide played an important role in increasing PAP amount deposited on the RGO/GC electrode compared to that on the bare GC electrode, which is due to that RGO has the large specific surface area. The results from the spectra of IR, ^{1}H NMR and ESR and the measurement of molecular weight demonstrated that PAP is an oligomer with the free radicals and exhibited good redox activity in a wide pH range from pH < 1–9.0 and can effectively catalyze xanthine oxidation due to the presence of the free radicals and the reversible redox groups in the copolymer chain. On the basis of the direct oxidation of xanthine on PAP, the PAP/RGO/GC electrode was used as a xanthine biosensor. The biosensor showed a linear range from 1.0 to 120 μM xanthine at pH 6.0 with a correction coefficient of 0.9965 and fast response to xanthine oxidation. The peak potential of xanthine oxidation shifted from 0.814 to 0.668 V as pH increased from 5.0 to 7.5.

1. Introduction

Electrocatalytic materials are very interesting and important in the electrochemical field since the catalyst plays an important role in lowering the activation energy of the rate-determining step; hence it accelerates the reaction rate. Whether a species can be catalyzed electrochemically or not is mainly dependent on the electrode material. The conducting polymers are a new kind of electrocatalytic material because they can be oxidized and reduced reversibly in the solutions, which plays an important role in transferring charges between interested species and the conducting polymer. Among the conducting polymers, polyaniline is one of the promising conducting polymers due to its high conductivity, good redox reversibility and high stability in aqueous solutions and air (MacDiarmid, 2001; Lee et al., 2006). These novel properties provide its potent applications in the electrochemical and biochemical fields. One of its applications is used as a catalyst or mediator to catalyze redox of several species (Luo et al., 2007; Eftekhari, 2010). Unfortunately, the experimental results demonstrated that polyaniline was essentially electrochemically inactive and its conductivity vanished at pH > 5 (Huang et al., 1986; Focke et al., 1987). Therefore, the catalytic application of polyaniline is confined by pH value. To improve its pH dependence of redox activity, the introduction of pH functional groups into polyaniline chain is a good way, which was performed via the copolymerization of aniline and aniline derivatives with pH functional groups such as *o*-aminophenol (Mu, 2004). The aniline copolymers with hydroxyl group have good pH dependence in a wide pH range (Mu, 2004, 2008) and therefore were used to catalyze oxidation of hydrogen peroxide (Chen et al., 2009) and NADH (Mu et al., 2009) and reduction of dichromate (Zhang et al., 2009) at higher pH values. Recently, we found that the product of pyrogallol oxidation carried very stable free radicals (Mu and Chen, 2012). Therefore, we tried to synthesize the copolymer of *o*-aminophenol and pyrogallol in the acidic solutions. However, their copolymerization rate is very slow at the bare platinum and glassy carbon (GC) electrodes. To overcome this problem, reduced graphene oxide (RGO) was used to modify GC electrode, which was employed to study the copolymerization of *o*-aminophenol and pyrogallol, because graphene has higher specific surface area and high conductivity. It is to be expected that the copolymer would carry hydroxyl groups and free radicals. In this case, the copolymer was used to test the electrocatalytic ability for biomolecules. It was found that the copolymer can catalyze oxidation of some biomolecules; and in particular, it can effectively catalyze oxidation of xanthine. Xanthine is an important intermediate of purine metabolism in human beings. Determination of xanthine level in blood and tissue is essential for diagnosis and medical management of various diseases like hyperuricemia, gout, xanthinuria and renal failure (Devi et al., 2011). Xanthine oxidation was generally carried out in the presence of xanthine oxidase (XOD) due to very high over potentials at the bare electrodes. Xanthine biosensors constructed using XOD were successfully used to detect xanthine (Agüi et al., 2006; Villalonga et al., 2007; Wu and Hu, 2007). The XOD modified glassy carbon (GC) paste electrode showed a wide linear range of 0.5–40 μM xanthine

* Corresponding author. Tel.: +86 514 7975590; fax: +86 514 7975244.
E-mail address: slmu@yzu.edu.cn (S. Mu).

0956-5663/$ - see front matter © 2013 Elsevier B.V. All rights reserved.
http://dx.doi.org/10.1016/j.bios.2013.03.036

(Kirgöz et al., 2004). In addition, on the basis of direct chemistry of XOD, xanthine biosensors fabricated using clay colloid (Li and Hu, 2003; Sun, 2006; Shan et al., 2007), multi-wall carbon nanotubes and laponite nanoparticles with flavine adenosine dinucleotide as immobilized materials showed a low detection limit of 0.1 (Gao et al., 2009) and 0.01 μM (Shan et al., 2009) xanthine. However, the above xanthine biosensors were fabricated using expensive XOD, and its activity decayed with time. Therefore research is very active in synthesis of new catalysts for direct oxidation of xanthine. Recent research work demonstrated that an ultra thin electropolymerized film of 2-amino-1,3,4-thiadiazole (p-ATD) modified GC electrode can effectively catalyze xanthine oxidation, which was successfully used for determination of xanthine in a linear range of 10–100 μM (Kalimuthu and John, 2010). In this work, we reported the electrochemical synthesis and characterization of PAP and xanthine detection based on its direct oxidation on the PAP/RGO/GC electrode.

2. Experimental

Methanol was high performance liquid chromatograph grade. Pyrogallol and other chemicals used were of analytical reagent grade. They were purchased from Sinopharm Chemical reagent Co., Ltd. Doubly distilled water was used to prepare all aqueous solutions. The pH values of the solutions were determined with a PXD-12 pH meter.

A glassy carbon (GC) disk electrode (3 mm diameter) was polished with alumina slurry of 0.3 μm diameter on a polishing cloth and then sonicated in a distilled water bath for 15 min before use. A 5 μL aqueous dispersion of graphene oxide (GO) sheets (0.05 wt%) was dropped on a GC disk that was then allowed to dry at 40 °C to form a GO/GC electrode. The GO/GC electrode was reduced at −1.0 V for 90 min in a 0.30 M phosphate buffer of pH 4.1 to form a RGO/GC electrode. A traditional three-electrode system, consisting of a RGO/GC working electrode, a platinum foil counter electrode and a saturated calomel reference electrode (SCE), was used for the electrochemical experiments that were performed on a CHI 407 workstation.

A PAP/RGO/graphite electrode was used to determine ESR spectrum of PAP because the appropriate GC fiber was not available. The ^{1}H NMR spectrum of the sample was conducted on a 600 MHz Bruker spectrometer at 301 K in dimethyl sulfoxide-d_6 (DMSO-d_6) in a 5-mm diameter NMR tube. A Bruker A300 spectrometer was used for the ESR measurement. The microwave power was set at 63.5 mW. The modulation amplitude was set at 1.0 G. The Bruker Company provides a *g*-factor maker with $S^{3/2}$. Its *g* factor is 1.9800 ± 0.0006. The molecular weight of the sample was measured by mass spectrometry, using a LCQ Deca XP Max mass analyzer with an ion source of electrospray ionization (ESI). The ESI-MS was in positive mode. PAP was dissolved in methanol, which was filtered with 0.45 μm syringe filters before injection into the column. The methanol solution containing PAP was dropped on a pressed KBr pellet and then dried; finally its IR spectrum was measured using a Bruker IFS 66/s spectrometer. The impedance measurements of the PAP/RGO/GC electrode were performed on an Autolab Nova 1.8 instrument. Frequency sweeps extended from 10^4 to 0.01 Hz using a sinusoidal perturbation signal of 10 mV, peak-to-peak. The image of PAP polymerized on the RGO/GC electrode was observed by a field emission scanning electron microscope (SEM) S-4800 II FE-SEM.

3. Results and discussion

3.1. Electrochemical synthesis and redox activity of poly (*o*-aminophenol-co-pyrogallol)

The electrochemical copolymerization of *o*-aminophenol and pyrogallol was first carried out using cyclic voltammetry method in a mixture containing 0.60 M H_2SO_4, 20 mM *o*-aminophenol and various concentrations of pyrogallol from 10 to 50 mM. Fig. 1A shows the cyclic voltammograms for electrolysis of a mixture containing 20 mM pyrogallol, using a GC electrode as a working electrode. An oxidation peak at 0.65 V occurs on curve 1 for the first cycle, and then its peak current decreases with an increasing number of cycles, accompanied with a shift of the peak potential towards the positive potential direction. This experimental phenomenon indicates that a product was formed on the GC electrode.

Fig. 1B shows the cyclic voltammograms for electrolysis of the same solution, but using a RGO/GC electrode instead of a GC electrode. Two oxidation peaks at 0.45 and 0.65 V occur on curve 1 for the first cycle. The difference between Fig. 1A and B is that a new oxidation peak at 0.45 V occurs on curve 1 in Fig. 1B and the second oxidation peak at 0.65 V shifts first to 0.80 V for the second cycle and then shifts back to 0.75 V for the third cycle. This experimental result is attributed to RGO that catalyzed the copolymerization of *o*-aminophenol and pyrogallol due to the presence of free radicals in RGO (Chen and Mu, 2011). Our experimental result revealed a fact that the peak current at 0.45 V in Fig. 1B increases with increasing pyrogallol concentration and is higher than that at 0.65 V when the concentration of pyrogallol increases to 50 mM. This indicates that the oxidation peak at 0.45 V is caused by pyrogallol oxidation. The PAP prepared with seven cycles was used to record cyclic voltammograms at various pH values (Fig. 1C,D). After electrolysis, it was found that the color of the product deposited on both electrodes is deep yellow.

The cyclic voltammograms of the PAP/RGO/GC and PAP/GC electrodes in 0.20 M H_2SO_4 (pH 0.7) are shown in curves 1 and 2 of Fig. 1C, respectively. There are two anodic shoulders at 0.40 and 0.50 V and their corresponding cathodic shoulders at 0.18 and 0.45 V on curve 1; they would be caused by the redox of –OH groups in the PAP chain. Fig. 1C shows that the area of curve 2 is much smaller than that of curve 1, even though both PAP films were prepared under the same experimental conditions except the different electrode materials used. In this case, the RGO/GC electrodes were used to synthesize PAP in this work. The different areas between curves 1 and 2 indicate that the product amount deposited on the RGO/GC electrode is much greater than that deposited on the GC electrode (about 18:1), which was mainly caused by the large specific surface area of RGO.

Fig. 1D shows the pH dependence of the redox activity of the PAP/RGO/GC electrode in a 0.30 M Na_2SO_4 solution. As can be seen from Fig. 1D, only one anodic peak at 0.43 V and its corresponding reduction peak at 0.28 V occurs on curve 1 at pH 4.0, which is quite different from that of curve 1 in Fig. 1C. This difference means that the redox behavior of PAP is related to pH value, i.e., the redox process of PAP needs the participation of protons, which is similar to the redox of polyaniline in aqueous solutions (Huang et al., 1986). As pH increases from 4.0 (curve 1) to 9.0 (curve 6), the redox peak potentials shift towards the negative potential direction and then disappears gradually. Judging from the area of the cyclic voltammograms, PAP still retains its redox activity at pH 9.0.

To prepare enough amount of PAP for its characterization, all samples used in following measurements of FTIR, ^{1}H NMR, ESR, and molecular weight were prepared under a constant potential of 0.85 V, in a mixture containing 20 mM pyrogallol, 20 mM *o*-aminophenol and 0.60 M H_2SO_4.

3.2. Characterization of poly(*o*-aminophenol-co-pyrogallol)

Fig. 2A shows the result of the molecular weight measurement. It is clear that a peak at 301 is the strongest one among peaks in Fig. 2A. On the basis of the *m*/*z* ratios of the other two peaks at 279 and 317, we can make sure that the *m*/*z* ratios of 279, 301, and 317 are attributed to $[M+H]^+$, $[M+Na]^+$, and $[M+K]^+$, respectively. Therefore, the molecular weight of PAP is 278. The Na^+ and K^+ arose from glass

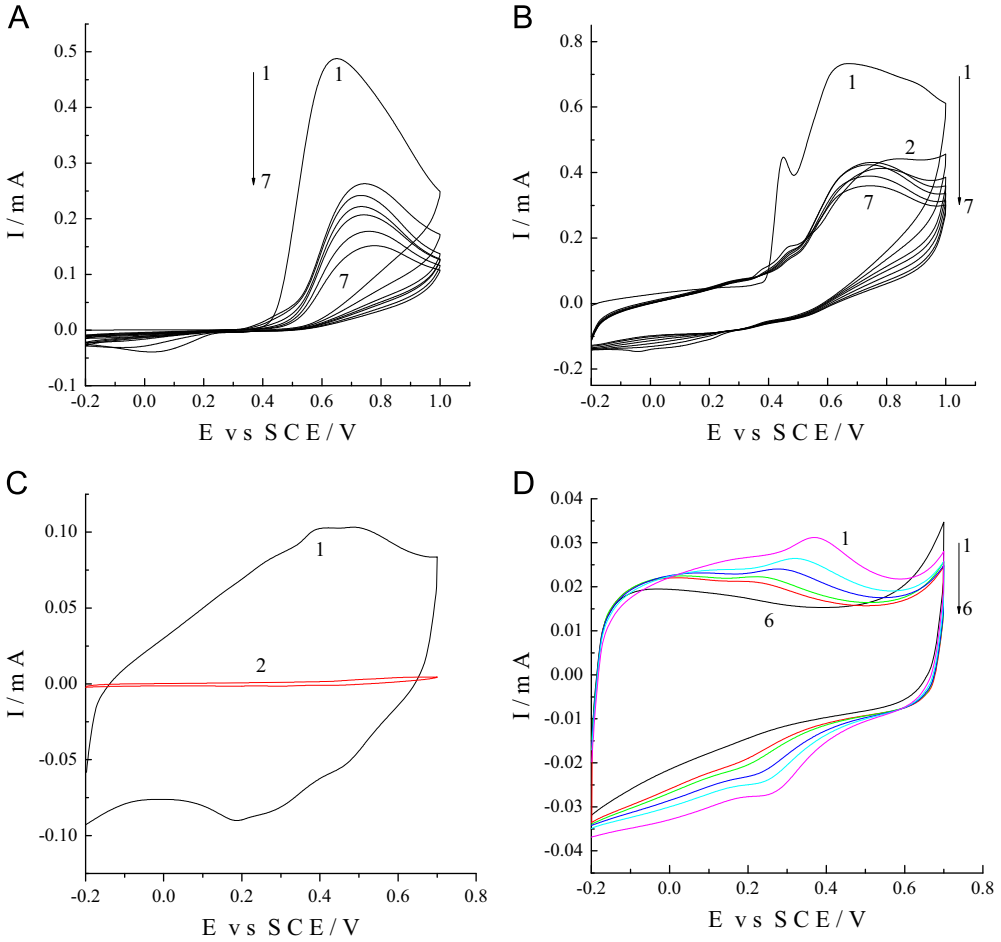

Fig. 1. The cyclic voltammograms for electrolysis of a mixture containing 20 mM pyrogallol, 20 mM *o*-aminophenol and 0.60 M H_2SO_4: (A) at a GC electrode; (B) at a RGO/GC electrode, curves: (1) first cycle, (7) seventh cycle. The cyclic voltammograms: (C) in a 0.20 M H_2SO_4 (pH 0.7) solution, (1) PAP/RGO/GC electrode, (2) PAP/GC electrode; (D) PAP/RGO/GC electrode in 0.30 M Na_2SO_4 solutions with various pH, (1) 4.0, (2) 5.0, (3) 6.0, (4) 7.0, (5) 8.0, (6) 9.0, at a scan rate of 60 mV s^{-1}.

containers used in the experiment. Such low molecular weight means that the copolymer is only an oligomer. In our case, the molecular formula of the molecular weight of 278 is suggested to be following:

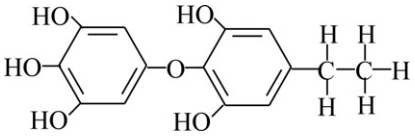

(1)

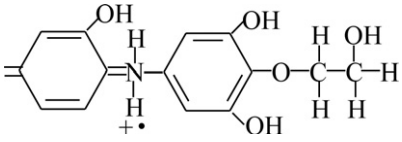

(2)

Formula (1) represents only polymerization of pyrogallol in the mixture containing pyrogallol and *o*-aminophenol, i.e., *o*-aminophenol did not take part in the polymerization in the electrolytic process. Formula (2) arises from the copolymerization of pyrogallol and *o*-aminophenol in the mixture. *o*-Aminophenol in the acidic solutions is first protonated as well as aniline in the acidic solutions (Huang et al., 1986).

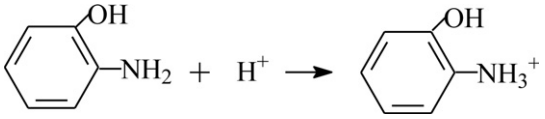

The cyclic voltammogram in Fig. 1B indicates that pyrogallol in the mixture was first oxidized when the potential swept from –0.20 V towards the positive potential direction. This gives us a hint that a dipolymer of pyrogallol would be first formed, then it was copolymerized with protonated *o*-aminophenol to form a tripolymer as the potential increased further and finally one of benzene rings of pyrogallol in the tripolymer was cleaved to form the resulting copolymer, i.e., Formula (2).

Fig. 2B shows the FTIR spectrum of PAP polymerized on a RGO/GC electrode. The main peaks are discussed here. A peak at 3652 cm^{-1} is assigned to O–H stretching vibrations. Two peaks at 3311 and 3171 $cm^{-1}$are attributed to N–H stretching vibrations. A broad band at 1735 cm^{-1} would be attributed to overtones and combinations of CH out-of-plane deformation in aromatic compounds (Lambert et al., 1998). The peaks at 1604 and 1491 cm^{-1} are attributed to C=C stretching vibrations of the quinone and benzene rings, respectively. A broad band at 1359 cm^{-1} is attributed to the C–O–H deformation vibrations because the C–O–H deformation in phenols is in the range 1390–1310 cm^{-1} (Lambert et al., 1998). A peak at 1026 cm^{-1} is attributed to the stretching vibrations of C–O in alcohols because its stretching vibration is in the range 1060–1025 cm^{-1} (Lambert et al., 1998). A peak at 915 cm^{-1} is attributed to out-of-plane CH deformations in aromatic compounds (Lambert et al., 1998). A peak at 714 cm^{-1} is assigned to OH out-of plane deformations in phenols (Lambert et al., 1998). The IR spectrum indicates the presence of N–H bond in the resulting product; however there is no N–H bond in

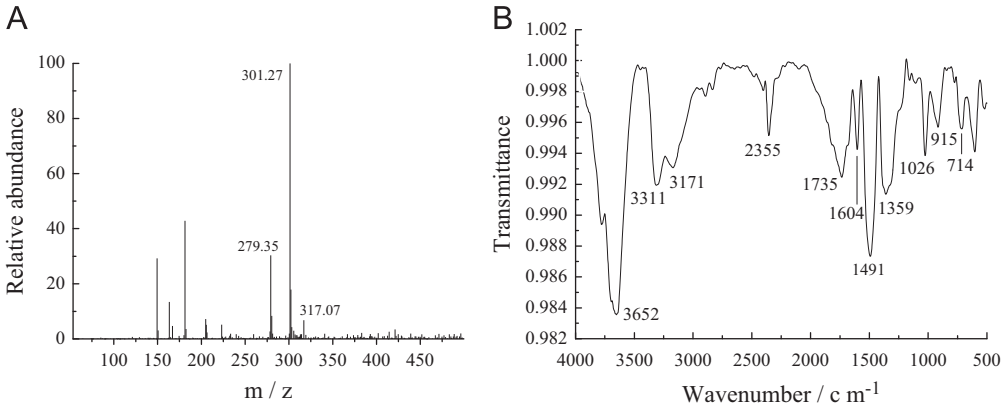

Fig. 2. (A) Mass spectrum (ESI-MS positive mode) of PAP dissolved in methanol and (B) FTIR spectrum of PAP dissolved in methanol that was dropped on a pressed KBr pellet.

Formula (1). This result indicates that the structure of the resulting product is Formula (2).

Fig. 3A is the electron spin resonance (ESR) spectrum of PAP polymerized on a RGO/graphite fiber, its *g* factor is 2.0037. This result indicates that the free radicals are contained in PAP.

Fig. 3B is the ^{1}H NMR spectrum of PAP, in which a 1/1/1 strong triplet with equally spaced lines at 7.186, 7.101 and 7.016 ppm is indicative of NH proton resonance due to the ^{14}N with unit spin, which makes the proton attached to it to split into three lines. This result is very similar to the ^{1}H NMR spectrum of polyaniline (Mu, 2010), in which the unpaired spins reside on a nitrogen atom (Long et al., 1993). A weak broad band from 6.6 to7.4 ppm is assigned to aromatic proton resonance of PAP because several nonequivalent protons in benzene and quinone rings of PAP would show the NMR signals with different chemical shifts. The presence of unpaired electrons as mentioned previously makes relaxation of protons in the benzene and quinone rings of PAP occur due to unpaired electrons having very large magnetic dipoles, which is more effective for relaxation process. As a result, several NMR lines merge into a broad single band in Fig. 3B. Fig. 3C shows the image of PAP deposited on the RGO/GC electrode, which consists of spherical particles with an average diameter of 70 nm.

3.3. Evidence for electrocatalytic oxidation of xanthine on the PAP electrode

Fig. 4A shows the cyclic voltammograms of RGO/GC and PAP/RGO/GC electrodes in the 0.20 M phosphate buffer of pH 6.0 with and without xanthine. Curves 1 and 2 are the cyclic voltammograms of the PAP/RGO/GC and RGO/GC electrodes in 0.20 M phosphate buffer, respectively. Curve 3 shows the cyclic voltammogram of RGO/GC electrode in 0.20 M phosphate buffer with 0.20 mM xanthine. Curves 4 and 5 show the cyclic voltammograms of the PAP/RGO/GC electrode in 0.20 M phosphate buffer containing 0.10 and 0.20 mM xanthine, respectively. Fig. 4 indicates that the oxidation current on curve 3 is higher than that on curve 2, indicating that xanthine was oxidized on the RGO/GC electrode, but no xanthine oxidation peak occurs on curve 3; however, a well defined oxidation peak occurs on curves 4 and 5, and its peak current increases with increasing xanthine concentration, indicating that this peak is caused by xanthine oxidation. Even though xanthine was oxidized at the RGO/GC electrode as discussed above, there is no oxidation peak at 0.75 V on curve 3, indicating that RGO cannot catalyze xanthine oxidation. The latter might be attributed to the slow charge transfer between xanthine and RGO.

To confirm the charge transfer rate of the PAP/RGO/GC electrode being faster than that of the RGO/GC electrode, the impedance measurements of both RGO/GC and PAP/RGO/GC electrodes were carried out in 0.20 M phosphate buffer containing 0.10 mM xanthine of pH 6.0. The potential was set at 0.75 V because that is the anodic peak potential of xanthine oxidation. Curves 1 and 2 in Fig. 4B are the impedance plots of the RGO/GC and PAP/RGO/GC electrodes, respectively. Clearly, the impedance of the PAP/RGO/GC electrode is lower than that of the RGO/GC electrode, indicating that the charge transfer rate of the PAP/RGO/GC electrode is faster than that of the RGO/GC electrode in the xanthine oxidation process. This result would be attributed to the PAP radical.

The reaction mechanism of xanthine oxidation on the PAP/RGO/GC electrode is suggested as follows. The radical is very active; therefore the radical of PAP would react with xanthine immediately to form xanthine radical:

$$[PAP]^{\bullet+} + Xanthine \rightarrow PAP + [Xanthine]^{\bullet+}$$

The xanthine radical was oxidized at the PAP/RGO/GC electrode as the potential swept to more positive direction:

$$[Xanthine]^{\bullet+} - e \rightarrow Uric\ acid + H_2O_2$$

This reaction rate would be faster than that of xanthine oxidation on the RGO/GC electrode because of no xanthine radical in the latter electrode. Therefore the concentration of xanthine at the PAP/RGO/GC electrode surface must drop more quickly than that on the RGO/GC electrode surface; hence its flux to the PAP/RGO/GC electrode increased. As a result, a pronounced oxidation peak occurs on curves 4 and 5 in Fig. 4A. In addition, we found that the copolymer can also catalyze oxidation of dopamine and uric acid in 0.20 M phosphate buffer of pH 6.0.

3.4. Determination of xanthine based on its direct oxidation on the PAP/RGO/GC electrode

Fig. 4A demonstrates that the anodic peak current increases with increasing xanthine concentration. To study further their relationship, linear sweep voltammetry was used to determine the change in the anodic peak current with xanthine concentration instead of cyclic voltammetry because xanthine oxidation is irreversible, evidence for this is that no corresponding cathodic peak occurs in Fig. 4A. In this section, PAP was prepared with four cycles between –0.20 and 0.90 V. Fig. 5A shows the linear sweep voltammograms of the PAP/RGO/GC electrode in the 0.20 M phosphate buffers with various xanthine concentrations of pH 6.0. The scan rate was set at 50 mV s^{-1}. In this experiment, after each measurement the electrode was rinsed with pH 6.0 phosphate buffer. The purpose for this is to remove the reactant and product residing on the electrode surface. Fig. 5A

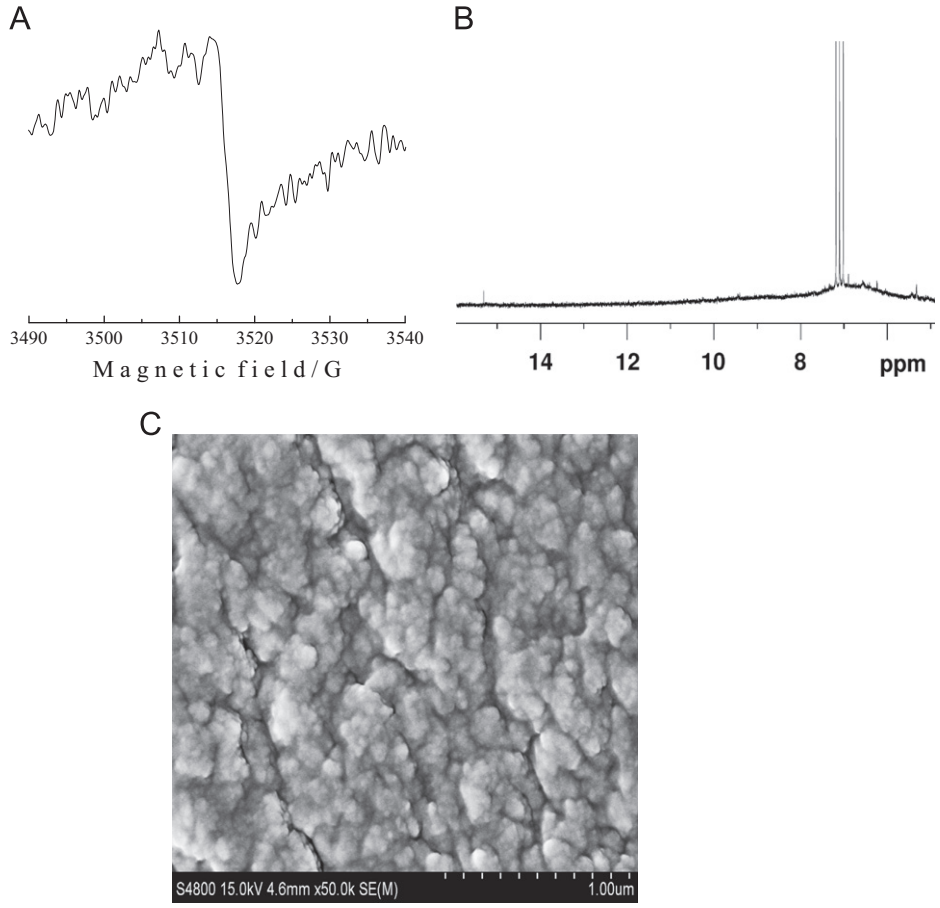

Fig. 3. (A) ESR spectrum of PAP, (B) ^{1}H NMR spectrum of PAP dissolved in DMSO-d_6 and (C) image of PAP polymerized on RGO/GC.

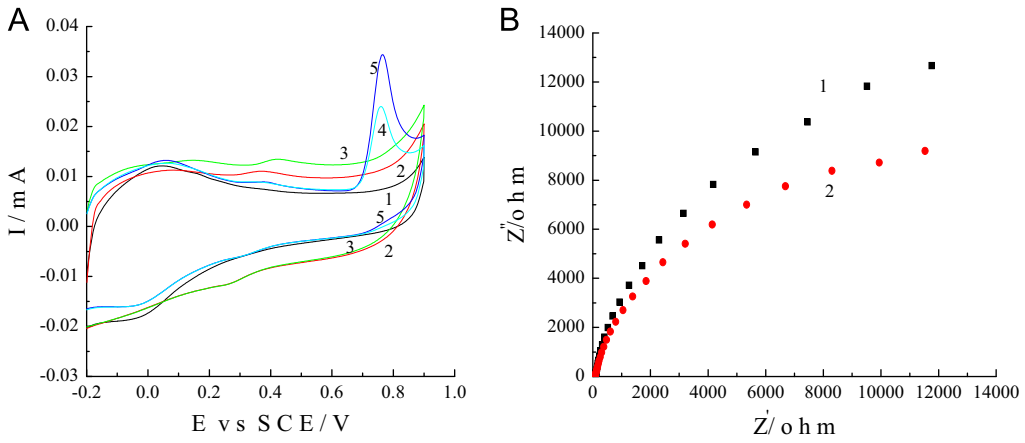

Fig. 4. (A) Cyclic voltammograms of the RGO/GC (curves 2 and 3) and PAP/RGO/GC (curves 1, 4, and 5) electrodes in 0.20 M phosphate buffer of pH 6.0 without and with xanthine, (1 and 2) without xanthine, (4) with 0.1 mM xanthine, (3 and 5) with 0.20 mM xanthine, at a scan rate of 20 mV s^{-1}; (B) The impedance plots in 0.20 M phosphate buffer containing 0.10 mM xanthine of pH 6.0: (1) RGO/GC electrode, (2) PAP/RGO/GC electrode, at 0.75 V.

indicates that an anodic peak at 0.75 V occurs on each curve. This peak potential is in agreement with that of p-ATD polymer, in which the peak potential was at 0.76 V (vs. NaCl saturated Ag/AgCl) (Kalimuthu and John, 2010). The net response current for xanthine oxidation was calculated from the anodic peak current minus the background current of the PAP/RGO/GC electrode in the 0.20 M phosphate buffers of pH 6.0 at 0.75 V. Fig. 5B shows the net response current as a function of xanthine concentration from 1.0 to 180 μM. The amperometric response to xanthine shows a linear range from 1.0 to 120 μM (inset of Fig. 5B) with a correction coefficient of 0.9965. The detection limit is 0.5 μM. The linear range reported here is wider than that of the p-ATD modified electrode (Kalimuthu and John, 2010).

Fig. 5C shows the effect of pH on the peak potential and peak current, in which the peak potential shifts from 0.814 to 0.668 V as pH increases from pH 5.0 to 7.5. This result gives us a hint that xanthine oxidation at the PAP/RGO/GC electrode liberated protons, which led to a shift of the peak potential towards the negative

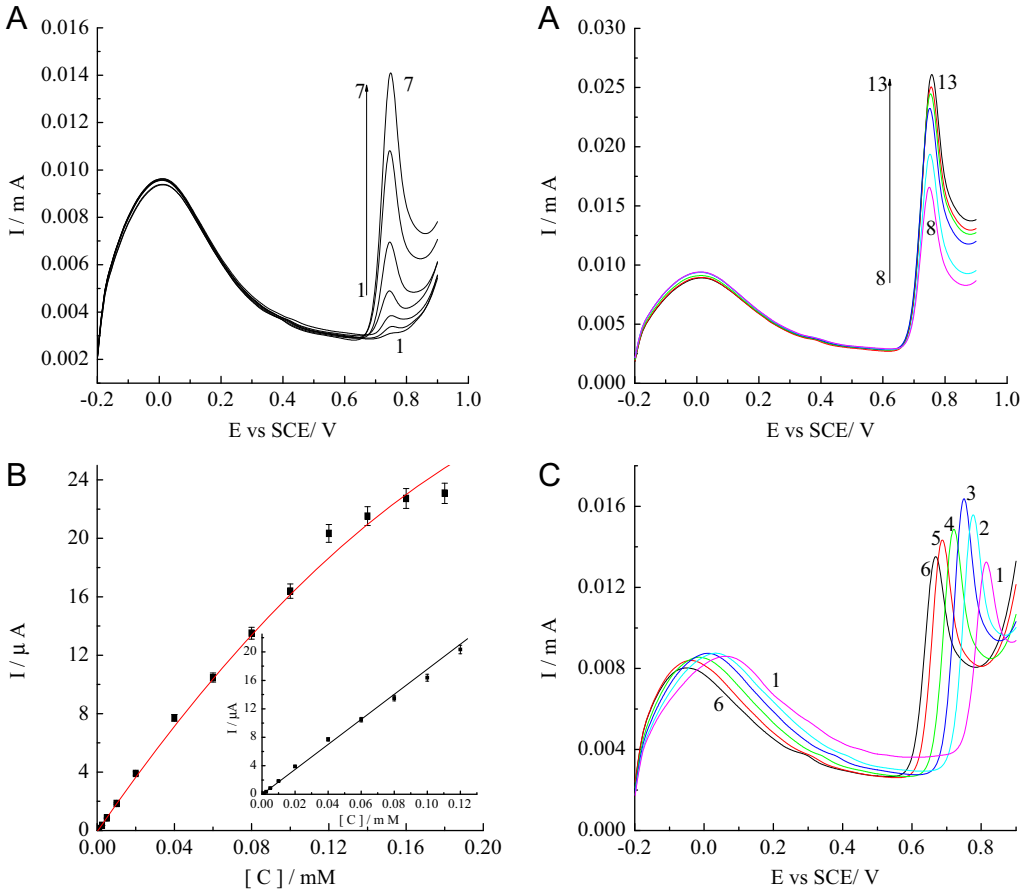

Fig. 5. Linear sweep voltammograms of the PAP/RGO/GC electrode in 0.20 M phosphate buffer containing xanthine at a scan rate of 50 mV s^{-1}. (A) In different xanthine concentrations of pH 6.0, (1) 0.001 mM, (2) 0.0025 mM, (3) 0.005 mM, (4) 0.01 mM, (5) 0.02 mM, (6) 0.04 mM, (7) 0.06 mM, (8) 0.08 mM, (9) 0.10 mM, (10) 0.12 mM, (11) 0.14 M, (12) 0.16 mM, (13) 0.18 mM. (B) The net response current as a function of xanthine concentration. (C) Voltammograms of the PAP/RGO/GC electrode in the buffer with 0.08 mM xanthine at different pH values, (1) 5.0, (2) 5.5, (3) 6.0, (4) 6.5, (5) 7.0, (6) 7.5.

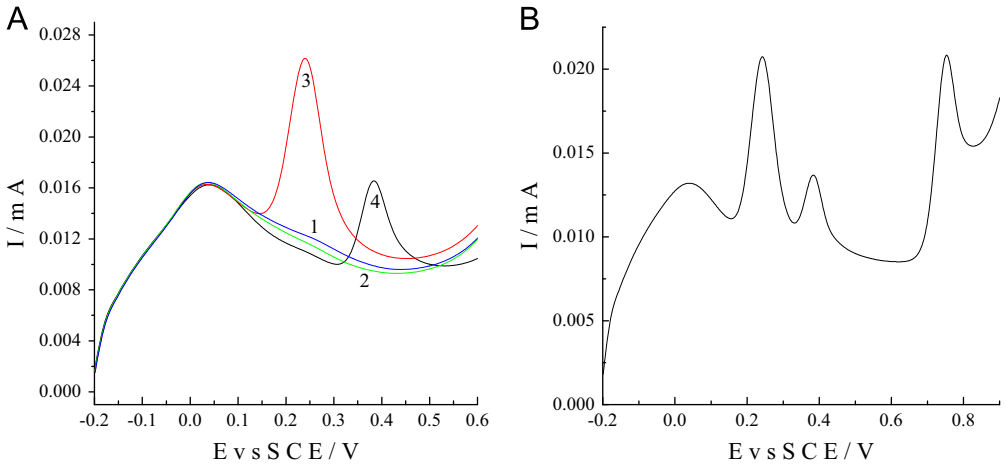

Fig. 6. Linear sweep voltammograms of the PAP/RGO/GC electrode in 0.20 M phosphate buffer with and without substrates, at pH 6.0 and a scan rate of 50 mV s^{-1}. (A): (1) in the buffer without substrate, (2) 0.10 mM ascorbic acid, (3) 0.10 mM dopamine, (4) 0.10 mM uric acid; (B) containing 0.10 mM of ascorbic acid, dopamine, uric acid and xanthine each.

direction as pH increased. This would be caused by the oxidation of hydrogen peroxide generated during the xanthine oxidation. The maximum peak current occurs at pH 6.0 in Fig. 5C.

The anti-interference characteristics of the PAP/RGO/GC electrode were performed in the phosphate buffer containing ascorbic acid, dopamine, and uric acid because they coexist with xanthine in human bodies. Fig. 6A shows that ascorbic acid cannot be oxidized (curve 2); however, the anodic peaks of dopamine and uric acid occur at 0.24 V (curve 3) and 0.38 V (curve 4), respectively. Fig. 5A shows the anodic peak of xanthine occurring at 0.75 V, therefore the oxidation potential of xanthine is 0.51 and 0.37 V more positive than that of dopamine and uric acid, respectively, indicating that ascorbic acid, dopamine and uric acid could not interfere with the measurement of xanthine. In order to

confirm this assumption, the linear voltammogram of the PAP/RGO/GC electrode in a mixture consisting of ascorbic acid, dopamine, uric acid and xanthine in the phosphate buffer is shown in Fig. 6B. Clearly, a well defined peak 4 occurs at 0.76 V that is caused by xanthine oxidation; and the anodic peaks 2, 3, and 4 are attributed to dopamine, uric acid and xanthine, respectively. Therefore, the results shown in Fig. 6 demonstrated that the presence of ascorbic acid, dopamine, and uric acid cannot interfere with the measurement of xanthine.

In this work, a same PAP/RGO/GC electrode was used for the characterization of its electrochemical property, measurements of xanthine concentration, and study on the pH dependence. After repeated measurements over 200 times during experimental course of about approximately 2 months, its activity showed a slight decay, but that can be recovered to a certain extent after cycling in acidic solution. In the consecutive measurements of three times, the average error is approximately 4%. On the basis of result from linear voltammogram from −0.20 to 0.90 V, a well defined oxidation peak of xanthine occurred at 0.82 V at a scan rate of 0.5 V s^{-1}, i.e., the response time was 2 s. Therefore, the PAP/RGO/GC electrode has very fast response to xanthine oxidation at pH 6.0.

4. Conclusions

In summary, poly(*o*-aminophenol-*co*-pyrogallol) was first synthesized via the electrochemical copolymerization of *o*-aminophenol and pyrogallol in the acidic solution, which is an oligomer proved by the molecular-weight determination. PAP was characterized using the electrochemical and spectroscopic methods; based on their result, the oligomer formula is presented in this paper. The cyclic voltammograms indicate that PAP has good redox activity in a wide pH range from pH <1 to pH 9.0 because of the hydroxyl groups in the copolymer. The experimental result demonstrated that PAP can effectively catalyze oxidation of xanthine, but the reduced graphene oxide cannot. Therefore, the PAP/RGO/GC electrode was used as a xanthine biosensor, which showed a linear response towards xanthine concentration between 1.0 and 120 μM at pH 6.0. Its activity showed slight decay after repeated measurements over 200 times; but that can be recovered to a certain extent after cycling in acidic solutions. The advantage of the xanthine biosensor reported here is that PAP was used as a catalyst instead of expensive XOD, and the biosensor has fast response and good stability.

Acknowledgments

This work is supported by Beijing National Laboratory for Molecular Sciences, 2012.

References

Agüi, L., Manso, J., Yáñez-Sedeño, P., Pingarrón, J.M., 2006. Sensors and Actuators B 113, 272–280.
Chen, C.X., Sun, C., Gao, Y.H, 2009. Electrochemistry Communications 11, 450–453.
Chen, W.L., Mu, S.L., 2011. Electrochimica Acta 56, 2284–2289.
Devi, R., Thakur, M., Pundir, C.S., 2011. Biosensors and Bioelectronics 26, 3420–3426.
Eftekhari, A., 2010. Nanostructured Conductive Polymers. A John Wiley and Sons, Ltd., Publication, United Kingdom, pp. 695–701.
Focke, W.W., Wnek, G.E., Wen, Y., 1987. Journal of Physical Chemistry 91, 5813–5818.
Gao, Y.S., Shen, C.P., Di, J.W., Tu, Y.F., 2009. Materials Science and Engineering C 29, 2213–2216.
Huang, W.S., Humphrey, B.D., MacDiarmid, A.G., 1986. Journal of the Chemical Society, Faraday Transactions 1 (82), 2385–2400.
Kalimuthu, P., John, S.A., 2010. Talanta 80, 1686–1691.
Kirgöz, Ü.A., Timur, S., Wang, J., Telefoncu, A., 2004. Electrochemistry Communications 6, 913–916.
Lambert, J.B., Shurvell, H.F., Lightner, D.A., Cooks, R.G., 1998. Organic Structural Spectroscopy. Prentice Hall Inc., Upper Saddle River, NJ, pp. 190–223.
Lee, K., Cho, S., Park, S.H., Heeger, A.J., Lee, C.W., Lee, S.H., 2006. Nature 441, 65–68.
Li, Z., Hu, N., 2003. Journal of Electroanalytical Chemistry 558, 155–165.
Long, S.M., Cromack, K.R., Epstein, A.J., Sun, Y., MacDiarmid, A.G., 1993. Synthetic Metals 55–57, 648–653.
Luo, X.L., Killard, A.J., Smyth, M.R., 2007. Chemistry—A European Journal 13, 2138–2141.
MacDiarmid, A.G., 2001. Angewandte Chemie International Edition 40, 2581–2590.
Mu, S.L., 2004. Synthetic Metals 143, 259–268.
Mu, S.L., 2008. Journal of Physical Chemistry B 112, 63446349.
Mu, S.L., Zhang, Y., Zhai, J.P., 2009. Electrochemistry Communications 11, 1960–1963.
Mu, S.L., Chen, C., 2012. Journal of Physical Chemistry C 116, 3065–3070.
Mu, S.L., 2010. Synthetic Metals 160, 1931–1937.
Shan, D., Han, E., Xue, H.G., Cosnier, S., 2007. Biomacromolecules 8, 3041–3046.
Shan, D., Wang, Y.N., Xue, H.G., Cosnier, S., Ding, S.N., 2009. Biosensors and Bioelectronics 24, 3556–3561.
Sun, H., 2006. Journal of Porous Materials 13, 393–397.
Villalonga, R., Matos, M., Cao, R., 2007. Electrochemistry Communications 9, 454–458.
Wu, Y.H., Hu, S.S., 2007. Analytica Chimica Acta 602, 181–186.
Zhang, Y., Li, Q., Tang, R., Hu, Q.C., Sun, L., Zhai, J.P., 2009. Applied Catalysis B: Environmental 92, 351356.